21

Natural gas properties and flow computation

Ivan Marić and Ivan Ivek
Ruđer Bošković Institute
Croatia

1. Introduction

Precise measurement of fluid flow rate is essential in commercial and in process control applications. The flow rate can be measured using different principles and devices (Baker, 2000, Miller, 1996): Orifice, Turbine, Venturi, Nozzle, Target, V-cone, Pitot, Multiport averaging, Elbow, Wedge, Laminar flow, Gilfo, Positive displacement, Thermal mass, Ultrasonic-time of flight, Variable area, Vortex, Coriolis. The measurement accuracy varies from ±5% of rate (Pitot) down to ±0.2% of rate (Coriolis). The Coriolis mass flowmeters are generally used to measure the mass flow of liquids but have been also used for the measurement of flow of high density gases. The turbine meters are widely used for the measurement of the volumetric flow rate of clean gases (±0.5% of rate) and liquids (±1% of rate). The flow rate measurements based on orifice meters are less accurate (1-2% URV) but the orifice plates are the most widely used devices in natural gas flow rate measurements due to their simplicity and robustness. We will here illustrate the thermodynamic effects that may cause significant error in measurements of natural gas flow rate based on orifice meters. We will also demonstrate how they could be efficiently compensated.
In measurements based on orifice plates the temperature of the fluid measured upstream of the orifice plate is used for the calculation of the flow rate but the fluid temperature is preferably measured downstream of the orifice plate (ISO-5167-1, 2003). When a gas is forced to flow through an orifice its temperature is changed due to the Joule-Thomson (JT) effect. The effect can be generally neglected for low flow rates i.e. for low differential pressures measured across the orifice meter (ISO-5167-1, 2003). At higher differential pressures and at lower temperatures the flow rate error increases and generally needs to be compensated (Marić, 2007). The precise compensation of flow rate error implies double calculation of natural gas properties and the flow rate, which extends the calculation time significantly and may become impractical for implementation in low-computing-power embedded systems. To avoid the computational burden the original high complexity models of natural gas properties can be replaced by the corresponding low-complexity surrogate models (Marić & Ivek, IEEE, Marić & Ivek, 2010) with no significant deterioration of flow rate accuracy.
Comprehensive presentation of modern methods of estimating the physical properties of gases and liquids can be found in (Poling at al., 2000). Formulations explicit in the Helmholtz energy have been widely used to represent the properties of natural gas because of the ease of calculating all other thermodynamic properties by mathematical

differentiation (Lemmon & Starling, 2003, Span & Wagner, 1996, Span & Wagner, 2003). The Helmholtz energy is a fundamental thermodynamic property from which all other thermodynamic properties can be calculated as derivatives with respect to molar density or temperature. The detailed procedure for the calculation of thermodynamic properties based on formulations explicit in Helmholtz energy (Lemmon & Starling, 2003) and on AGA-8 detail characterization equation (Starling & Savidge, 1992) is given in (ISO-207651-1, 2005). Here we will elaborate an alternative procedure for the calculation of properties of a natural gas that was originally published in the Journal Flow Measurement and Instrumentation (Marić, 2005 & 2007). The procedure is derived using fundamental thermodynamic equations (Olander, 2007), DIPPR AIChE (DIPPR® Project 801, 2005) generic ideal heat capacity equations, and AGA-8 (Starling & Savidge, 1992) extended virial-type equations of state. The procedure specifies the calculation of specific heat capacities at a constant pressure c_p and at a constant volume c_v, the JT coefficient μ_{JT}, and the isentropic exponent κ of a natural gas. The effect of a JT expansion on the accuracy of natural gas flow rate measurements will be pointed out.
The possibilities of using the computational intelligence methods - Artificial Neural Networks - ANNs (Ferrari & Stengel, 2005, Wilamowski et al., 2008) and machine learning tools - Group Method of Data Handling - GMDH (Ivakhnenko, 1971, Nikolaev & Iba, 2003) for meta-modeling the effects of natural gas properties in flow rate measurements (Marić & Ivek, 2010) will be illustrated. The practical examples of ANN and GMDH surrogate models for the compensation of natural gas flow rate measurement error caused by the thermodynamic effects, with the corresponding accuracies and execution times will be given. The models are particularly suitable for implementation in low computing power embedded systems.

2. A procedure for the calculation of thermodynamic properties of natural gas

This section summarizes the procedure (Maric, 2007) for the calculation of specific heat capacity at constant pressure c_p and at constant volume c_v, JT coefficient μ_{JT} and isentropic exponent κ of a natural gas based on thermodynamic equations, AGA-8 extended virial type characterization equation (Starling & Savidge, 1992, ISO-12213-2, 2006) and DIPPR generic ideal heat capacity equations (DIPPR® Project 801, 2005). First, the relation of the molar heat capacity at constant volume to equation of state will be derived. Then the relation will be used to calculate a molar heat capacity at constant pressure, which will be then used for the calculation of the JT coefficient and the isentropic exponent. The total differential for entropy (Olander, 2007), related to temperature and molar volume, is:

$$ds = \left(\frac{\partial s}{\partial T}\right)_{v_m} dT + \left(\frac{\partial s}{\partial v_m}\right)_T dv_m \,, \tag{1}$$

where s denotes entropy, T denotes temperature and v_m is a molar volume of a gas. By dividing the fundamental differential for internal energy $du = T \cdot ds - p \cdot dv_m$ by dT while holding v_m constant the coefficient of dT in Eq. (1) becomes $c_{m,v}/T$ since the molar heat at constant volume is defined by $c_{m,v} = \left(\partial u/\partial T\right)_{v_m}$. The Maxwell relation

$\left(\partial s/\partial v_m\right)_T = \left(\partial p/\partial T\right)_{v_m}$, is used to substitute the coefficient of dv_m. Finally, the Eq. (1) becomes:

$$ds = \frac{c_{m,v}}{T} dT + \left(\frac{\partial p}{\partial T}\right)_{v_m} dv_m \,. \tag{2}$$

Similarly, starting from a total differential for entropy related to temperature and pressure (Olander, 2007) $ds = \left(\partial s/\partial T\right)_p dT + \left(\partial s/\partial p\right)_T dp$ and by dividing the fundamental differential for enthalpy $dh = T \cdot ds + v_m \cdot dp$ by dT while holding p constant, the coefficient of dT in total differential becomes $c_{m,p}/T$ since the molar heat capacity at constant pressure is defined by: $c_{m,p} = \left(\partial h/\partial T\right)_p$. The Maxwell relation $\left(\partial s/\partial p\right)_T = \left(\partial v_m/\partial T\right)_p$ is used to substitute the coefficient of dp and the following relation is obtained:

$$ds = \frac{c_{m,p}}{T} dT + \left(\frac{\partial v_m}{\partial T}\right)_p dp \,, \tag{3}$$

Subtracting Eq. (2) from Eq. (3), then dividing the resulting equation by dv_m while holding p constant and finally inverting the partial derivative $\left(\partial T/\partial v_m\right)_p$ the following equation is obtained:

$$c_{m,p} - c_{m,v} = T\left(\frac{\partial v_m}{\partial T}\right)_p \left(\frac{\partial p}{\partial T}\right)_{v_m} \,. \tag{4}$$

A total differential of thermodynamic property, Eqs. (2) and (3), must be the exact differential i.e. the order of forming the mixed second derivative is irrelevant. The partial derivative of the first coefficient with respect to the second variable equals to the partial derivative of the second coefficient with respect to the first variable. By applying this property to Eq. (2) and by assuming T to be the first variable with the corresponding coefficient $c_{m,v}/T$ and v_m the second variable with the corresponding coefficient $\left(\partial p/\partial T\right)_{v_m}$ we obtain:

$$\left(\frac{\partial c_{m,v}}{\partial v_m}\right)_T = T\left(\frac{\partial^2 p}{\partial T^2}\right)_{v_m} \,, \tag{5}$$

The Eq. (5) can be rewritten in the following integral form:

$$c_{m,v} = c_{m,vI} + T \int_{v_{mI}\to\infty(T=const)}^{v_m} \left(\frac{\partial^2 p}{\partial T^2}\right)_{v_m} dv_m \,, \tag{6}$$

where $c_{m,vI}$, v_{mI} and v_m denote the ideal molar heat capacity at constant volume and the corresponding molar volume of ideal and real gas at temperature *T*. Real gases behave more like ideal gases as pressure approaches zero or $v_{mI} \to \infty$. After substituting $v_m = 1/\rho_m$, $p = RTZ\rho_m$ and $c_{m,vI} = c_{m,pI} - R$ the Eq. (6) transforms to:

$$c_{m,v} = c_{m,pI} - R - RT \int_{\rho_{mI}\to 0(T=const)}^{\rho_m} \frac{1}{\rho_m}\left(2\left(\frac{\partial Z}{\partial T}\right)_{\rho_m} + T\left(\frac{\partial^2 Z}{\partial T^2}\right)_{\rho_m}\right) d\rho_m \,, \tag{7}$$

where $c_{m,pI}$ denotes the temperature dependent molar heat capacity of ideal gas at constant pressure, *R* is the universal gas constant, *Z* is the compression factor and ρ_{mI} and ρ_m are the corresponding molar densities of ideal and real gas at temperature *T*. After substituting the first and the second derivative of the AGA-8 compressibility equation (Starling & Savidge, 1992, ISO-12213-2, 2006)

$$Z = 1 + B\rho_m - \rho_r \sum_{n=13}^{18} C_n^* + \sum_{n=13}^{58} C_n^* \left(b_n - c_n k_n \rho_r^{k_n}\right) \rho_r^{b_n} e^{-c_n \rho_r^{k_n}} \,, \tag{8}$$

into the Eq. (7) and after integration we obtain

$$c_{m,v} = c_{m,pI} - R + RT\rho_r \left(2C_0 + TC_1 - C_2\right), \tag{9}$$

with

$$C_0 = \sum_{n=13}^{18} C_n^{*\prime} - \frac{B'}{K^3} \,, \tag{10}$$

$$C_1 = \sum_{n=13}^{18} C_n^{*\prime\prime} - \frac{B''}{K^3} \,, \tag{11}$$

$$C_2 = \sum_{n=13}^{58} \left(2C_n^{*\prime} + TC_n^{*\prime\prime}\right) \rho_r^{b_n - 1} e^{-c_n \rho_r^{k_n}} \,, \tag{12}$$

where ρ_r is the reduced density ($\rho_r = K^3\rho_m$), B is the second virial coefficient, $\{C_n^*\}$ are the temperature dependent coefficients, K is the mixture size parameter while $\{b_n\}$, $\{c_n\}$ and $\{k_n\}$ are the equation of state parameters. The mixture size parameter K is calculated using the following equation (ISO-12213-2, 2006):

$$K^5 = \left(\sum_{i=1}^{N} y_i K_i^{5/2}\right)^2 + 2\sum_{i=1}^{N-1}\sum_{j=i+1}^{N} y_i y_j (K_{ij}^5 - 1)(K_i K_j)^{5/2}, \tag{13}$$

where y_i denotes the molar fraction of the component i, while $\{K_i\}$ and $\{K_{ij}\}$ are the corresponding size parameters and the binary interaction parameters given in [ISO-12213-2, 2006]. According to (ISO-12213-2, 2006) the second virial coefficient is calculated using the following equation:

$$B = \sum_{n=1}^{18} a_n T^{-u_n} \sum_{i=1}^{N}\sum_{j=1}^{N} y_i y_j B_{nij}^* E_{ij}^{u_n} (K_i K_j)^{3/2}, \tag{14}$$

and the coefficients $\{B_{nij}^*\}$, $\{E_{ij}\}$ and $\{G_{ij}\}$ are defined by

$$\begin{aligned} B_{nij}^* = {} & (G_{ij} + 1 - g_n)^{g_n} (Q_i Q_j + 1 - q_n)^{q_n} (F_i^{1/2} F_j^{1/2} + 1 - f_n)^{f_n} \cdot \\ & \cdot (S_i S_j + 1 - s_n)^{s_n} (W_i W_j + 1 - w_n)^{w_n} \end{aligned}, \tag{15}$$

$$E_{ij} = E_{ij}^* (E_i E_j)^{1/2}, \tag{16}$$

and

$$G_{ij} = G_{ij}^* (G_i + G_j)/2, \tag{17}$$

where T is temperature, N is the total number of gas mixture components, y_i is the molar fraction of the component i, $\{a_n\}$, $\{f_n\}$, $\{g_n\}$, $\{q_n\}$, $\{s_n\}$, $\{u_n\}$, and $\{w_n\}$ are the equation of state parameters, $\{E_i\}$, $\{F_i\}$, $\{G_i\}$, $\{K_i\}$, $\{Q_i\}$, $\{S_i\}$ and $\{W_i\}$ are the corresponding characterization parameters while $\{E_{ij}^*\}$ and $\{G_{ij}^*\}$ are the corresponding binary interaction parameters. The main symbols and units are given in Table 1.

The temperature dependent coefficients $\{C_n^*; n = 1,...,58\}$ and the mixture parameters U, G, Q and F are calculated using the equations (ISO-12213-2, 2006):

$$C_n^* = a_n (G + 1 - g_n)^{g_n} (Q^2 + 1 - q_n)^{q_n} (F + 1 - f_n)^{f_n} U^{u_n} T^{-u_n}, \tag{18}$$

Symbols and units		
Symbol	**Description**	**Unit**
B	Second virial coefficient	m^3*kmol^{-1}
B^*_{nij}	Mixture interaction coefficient	-
C	Coefficient of discharge	-
$c_{m,p}$	Molar heat capacity at constant pressure	J/(mol·K)
$c_{m,v}$	Molar heat capacity at constant volume	J/(mol·K)
C^*_n	Temperature and composition dependent coefficients	-
c_n	AGA-8 equation of state parameter	-
c_p	Specific heat capacity at constant pressure	J/(kg·K)
$c_{m,pI}$	Ideal molar heat capacity of the natural gas mixture	J/(mol·K)
$c^j_{m,pi}$	Ideal molar heat capacity of the gas component j	J/(mol·K)
D	Upstream internal pipe diameter	m
d	Diameter of orifice	m
h	Specific enthalpy	J/kg
K	Size parameter	-
M	Molar mass of the gas mixture	kg·kmol^{-1}
p	Absolute pressure	Pa
q	Mass flow rate	kg/s
R	Molar gas constant 8314.51	J/(kmol·K)
s	Specific entropy	J/(kg·K)
T	Absolute temperature	K
v_m	Molar specific volume	m^3/kmol
v_{mI}	Molar specific volume of ideal gas	m^3/kmol
y_i	Molar fraction of i-th component in gas mixture	-
Z	Compression factor	-
β	Diameter ratio d/D	-
Δp	Differential pressure	Pa
$\Delta\omega$	Pressure loss	Pa
κ	Isentropic exponent	-
μ_{JT}	Joule-Thomson coefficient	K/Pa
ρ_m	Molar density	kmol/m^3
ρ_{mI}	Molar density of ideal gas	kmol/m^3
ρ_r	Reduced density	-

Table 1. Symbols and units (for additional symbols and units refer to (ISO-12213-2, 2006).

$$U^5 = \left(\sum_{i=1}^{N} y_i E_i^{5/2} \right)^2 + 2 \sum_{i=1}^{N-1} \sum_{j=i+1}^{N} y_i y_j (U_{ij}^5 - 1)(E_i E_j)^{5/2}, \tag{19}$$

$$G = \sum_{i=1}^{N} y_i G_i + 2 \sum_{i=1}^{N-1} \sum_{j=i+1}^{N} y_i y_j (G_{ij}^* - 1)(G_i + G_j), \tag{20}$$

$$Q = \sum_{i=1}^{N} y_i Q_i, \tag{21}$$

and

$$F = \sum_{i=1}^{N} y_i^2 F_i \,, \tag{22}$$

where, U_{ij} is the binary interaction parameter for mixture energy. The first and the second derivatives of the coefficients *B* and C_n^*, with respect to temperature are:

$$B' = -\sum_{n=1}^{18} a_n u_n T^{-u_n-1} \sum_{i=1}^{N}\sum_{j=1}^{N} y_i y_j B_{nij}^* E_{ij}^{u_n} (K_i K_j)^{3/2} \,, \tag{23}$$

$$B'' = \sum_{n=1}^{18} a_n u_n (u_n+1) T^{-u_n-2} \sum_{i=1}^{N}\sum_{j=1}^{N} y_i y_j B_{nij}^* E_{ij}^{u_n} (K_i K_j)^{3/2} \,, \tag{24}$$

$$C_n^{*'} = -\frac{u_n}{T} C_n^* \,, \tag{25}$$

$$C_n^{*''} = -\frac{u_n+1}{T} C_n^{*'} \,, \tag{26}$$

The ideal molar heat capacity c_{pI} is calculated by

$$c_{m,pI} = \sum_{j=1}^{N} y_j c_{m,pi}^j \,, \tag{27}$$

where y_j is the molar fraction of component *j* in the gas mixture and $c_{m,pi}^j$ is the molar heat capacity of the same component. The molar heat capacities of the ideal gas mixture components can be approximated by DIPPR/AIChE generic equations (DIPPR® Project 801, 2005), i.e.

$$c_{m,pi}^j = a_j + b_j \left(\frac{c_j / T}{\sinh(c_j / T)} \right)^2 + d_j \left(\frac{e_j / T}{\cosh(e_j / T)} \right)^2 \,, \tag{28}$$

where $c_{m,pi}^j$ is the molar heat capacity of the component *j* of the ideal gas mixture, a_j, b_j, c_j, d_j and e_j are the corresponding constants, and *T* is the temperature.

The partial derivative of pressure with respect to temperature at constant molar volume and the partial derivative of molar volume with respect to temperature at constant pressure are defined by the equations:

$$\left(\frac{\partial p}{\partial T}\right)_{v_m} = R\rho_m\left[Z + T\left(C_3 - \rho_r C_0\right)\right], \tag{29}$$

and

$$\left(\frac{\partial v_m}{\partial T}\right)_p = \frac{R}{p}\left[Z + \left(\frac{\partial Z}{\partial T}\right)_p T\right], \tag{30}$$

where,

$$C_3 = \sum_{n=13}^{58}\left(C_n^{*'} D_n^*\right), \tag{31}$$

$$D_n = \left(b_n - c_n k_n \rho_r^{k_n}\right)\rho_r^{b_n} e^{-c_n \rho_r^{k_n}}, \tag{32}$$

$$\left(\frac{\partial Z}{\partial T}\right)_p = \frac{R(TZ)^2 C_3 - pZ\left[TK^3 C_0 + C_4\right]}{R(TZ)^2 + pTC_4}, \tag{33}$$

$$C_4 = C_5 + \sum_{n=13}^{58} C_n^* D_{1n}, \tag{34}$$

$$C_5 = B - K^3 \sum_{n=13}^{18} C_n^* \tag{35}$$

and

$$D_{1n} = K^3\left[b_n^2 - c_n k_n\left(2b_n + k_n - c_n k_n \rho_r^{k_n}\right)\rho_r^{k_n}\right]\rho_r^{b_n - 1} e^{-c_n \rho_r^{k_n}} \tag{36}$$

The isentropic exponent is defined by the following relation

$$\kappa = -\frac{c_{m,p}}{c_{m,v}}\left(\frac{\partial p}{\partial v_m}\right)_T\left(\frac{v_m}{p}\right) = -\frac{c_{m,p}}{c_{m,v}\rho_m p}\left(\frac{\partial p}{\partial v_m}\right)_T \tag{37}$$

where

$$\left(\frac{\partial p}{\partial v_m}\right)_T = \left(\frac{\partial p}{\partial \rho_m}\right)_T \left(\frac{\partial \rho_m}{\partial v_m}\right)_T = -RT\rho_m^2\left(Z + \rho_m C_4\right) \tag{38}$$

The JT coefficient is defined by the following equation:

$$\mu_{JT} = \frac{RT^2}{pc_{m,p}}\left(\frac{\partial Z}{\partial T}\right)_p \tag{39}$$

The derivation of the Eq. (39) is elaborated in (Olander, 2007 & Maric, 2005).

3. Implementation in software

The procedure for the calculation of natural gas density, compression, molar heat capacity, isentropic exponent and the JT coefficient can be implemented in object oriented paradigm, which enables its easy integration into the software projects. The interface to the software object *S* is shown in Fig. 1. The input/output parameters and functions are accessible while the internal structure is hidden to the user. The function "*Calculate*" maps the input parameters (pressure, temperature and the molar fractions of natural gas components) into the output parameters (density, compression, molar heat capacity, isentropic exponent, JT coefficient, etc.).

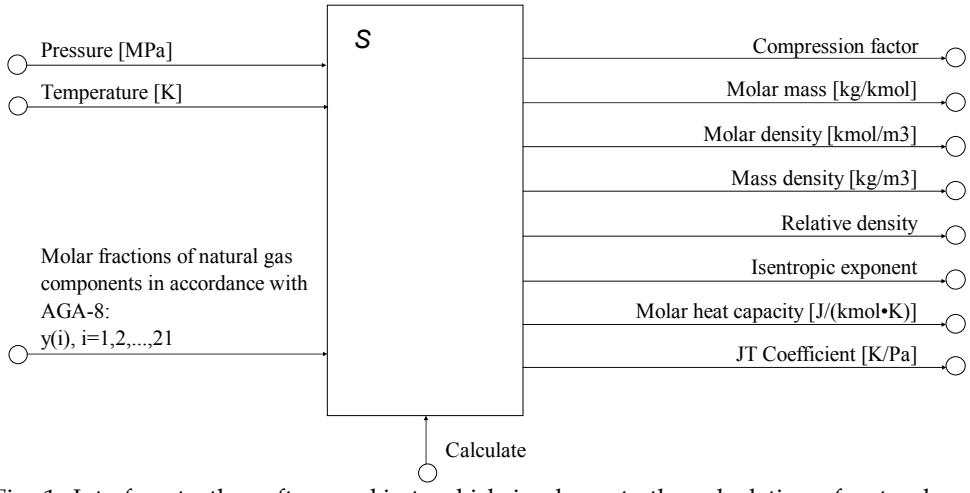

Fig. 1. Interface to the software object, which implements the calculation of natural gas properties.

Table 2 depicts the calculation procedure. Prior to the calculation of the molar heat capacities, isentropic exponent and JT coefficient, the density and the compression factor of a natural gas must be calculated. The false position method is combined with the successive bisection method to calculate the roots of the equation of state [Starling & Savidge, 1992].

Input parameters – constant:

- molar gas constant (R=8314.51 J/(kmol·K))
- natural gas equation of state parameters (a_n, b_n, c_n, k_n, u_n, g_n, q_n, f_n, s_n, w_n; n=1, 2,...,58), characterization parameters (M_i, E_i, K_i, G_i, Q_i, F_i, S_i, W_i; i=1,...,21) and binary interaction parameters ($E^*_{i,j}$, $U_{i,j}$, $K_{i,j}$, $G^*_{i,j}$) (see ISO 12213-2)
- DIPPR/AIChE gas heat capacity constants (a_j, b_j, c_j, d_j, e_j; j=1,2,...,N)

Input parameters – time varying:

- absolute pressure: p [MPa]
- absolute temperature: T [K]
- molar fractions of the natural gas mixture: y_i; i=1,2,...,N

Calculation procedure:

1. mixture size parameter K (Eq. 13), second virial coefficient B (Eq. 14) and temperature dependent coefficients C^*_n (Eq. 18)
2. compression factor Z (Eq. 8) (see ISO-12213-2 for details of calculation)
3. molar density $\rho_m = p/RTZ$, density $\rho = M\rho_m$, reduced density $\rho_r = K^3\rho_m$ and molar volume $v_m = 1/\rho_m$.
4. coefficients D_n and D_{1n} (Eqs. 32 and 36)
5. 1st and 2nd derivative of the second virial coefficient B: B' (Eq. 23) and B'' (Eq. 24)
6. 1st and 2nd derivative of the coefficient C^*_n: $C^{*\prime}_n$ (Eq. 25) and $C^{*\prime\prime}_n$ (Eq. 26)
7. 1st derivative of the compression factor Z: $\left(\partial Z/\partial T\right)_p$ (Eq. 33)
8. partial derivatives of pressure: $\left(\partial p/\partial T\right)_{v_m}$ (Eq. 29) and $\left(\partial p/\partial v_m\right)_T$ (Eq. 38)
9. ideal molar heat capacity of a gas mixture at constant pressure: $c_{m,pI}$ (Eq. 27)
10. molar heat capacity of a gas mixture at constant volume: $c_{m,v}$ (Eqs. 9)
11. molar heat capacity of a gas mixture at constant pressure: $c_{m,p}$ (Eqs. 4)
12. isentropic exponent κ (Eq. 37)
13. Joule-Thomson coefficient μ_{JT} (Eq. 39)

Table 2. The input/output parameters and the procedure for the computation of the natural gas properties.

4. Comparison with experimental results

In order to compare the calculation results, for the specific heat capacity c_p and the JT coefficient μ_{JT}, with the corresponding high accuracy measurement data (Ernst et al., 2001), we assume the identical artificial natural gas mixture with the following mole fractions: x_{CH4}=0.79942, x_{C2H6}=0.05029, x_{C3H8}=0.03000, x_{CO2}=0.02090 and x_{N2}=0.09939. The results of the measurements (Ernst et al., 2001) and the results of the calculation of the specific heat capacity c_p and the JT coefficient μ_{JT} of the natural gas mixture, for absolute pressure ranging from 0 MPa to 30 MPa in 0.5 MPa steps and for four upstream temperatures (250 K, 275 K, 300 K and 350 K), are shown in Fig. 2 and 3, respectively. The differences between the calculated values and the corresponding measurement results (Ernst et al., 2001), for the c_p and μ_{JT}, are shown in Table 3 and 4, respectively.

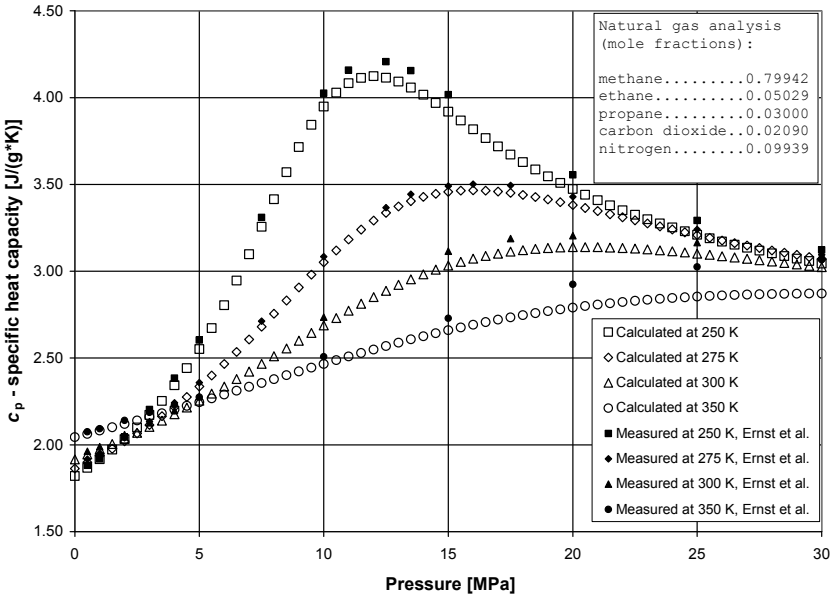

Fig. 2. Calculated and measured molar heat capacity at constant pressure of the natural gas mixture.

From Table 3 it can be seen that the calculated values of c_p are within ±0.08 J/(g*K) with the measurement results for the pressures up to 12 MPa. At higher pressures, up to 30 MPa, the difference increases but never exceeds ±0.2 J/(g*K). For pressures up to 12 MPa the relative difference between the calculated and experimentally obtained c_p never exceeds ±2.00%.

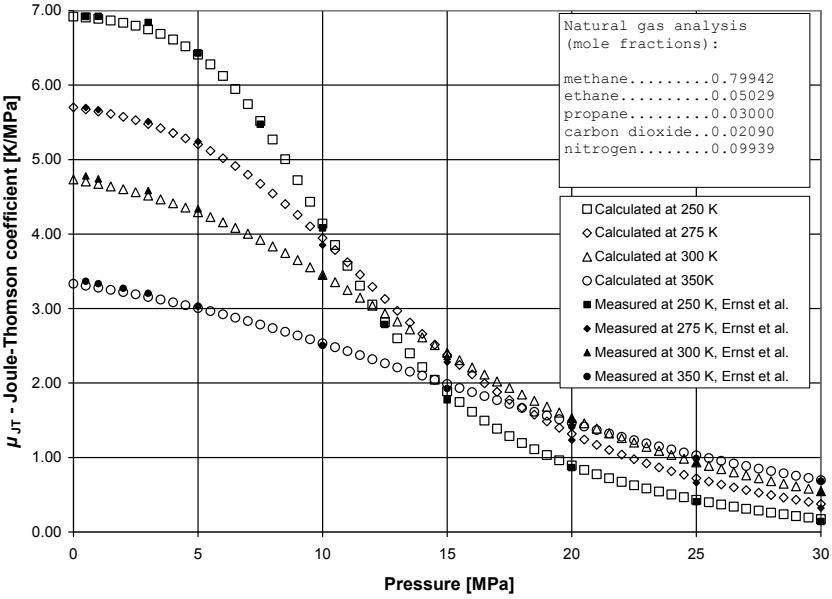

Fig. 3. Calculated and measured JT coefficient of the natural gas mixture.

P [MPa]: T [K]	250	275	300	350
	($c_{p\_calculated}$ - $c_{p\_measured}$) [J/(g*K)]			
0.5	-0.015	-0.018	-0.018	-0.012
1.0	-0.002	-0.014	-0.016	-0.011
2.0	-0.012	-0.019	-0.022	-0.020
3.0	-0.032	-0.020	-0.023	-0.026
4.0	-0.041	-0.023	-0.021	-0.027
5.0	-0.051	-0.022	-0.025	-0.029
7.5	-0.055	-0.032	-	-
10.0	-0.077	-0.033	-0.048	-0.042
11.0	-0.075	-	-	-
12.5	-0.092	-0.030	-	-
13.5	-0.097	-0.039	-	-
15.0	-0.098	-0.033	-0.082	-0.069
16.0	-	-0.036	-	-
17.5	-	-0.043	-0.075	-
20.0	-0.081	-0.048	-0.066	-0.134
25.0	-0.082	-0.033	-0.064	-0.171
30.0	-0.077	-0.025	-0.070	-0.194

Table 3. Difference between the calculated and measured specific heat capacity at constant pressure of a natural gas.

P [MPa]: T [K]	250	275	300	350
	$(\mu_{JT\_calculated} - \mu_{JT\_measured})$ [K/MPa]			
0.5	-0.014	-0.023	-0.075	-0.059
1.0	-0.032	-0.024	-0.068	-0.053
2.0	-	-	-	-0.051
3.0	-0.092	-0.032	-0.069	-0.049
5.0	-0.022	-0.036	-0.044	-0.026
7.5	0.043	-	-	-
10.0	0.060	0.096	0.019	0.030
12.5	0.034	-	-	-
15.0	0.113	0.093	0.050	0.061
20.0	0.029	0.084	0.009	0.047
25.0	0.025	0.059	0.002	0.043
30.0	0.031	0.052	0.005	0.012

Table 4. Difference between the calculated and measured JT coefficient of a natural gas.

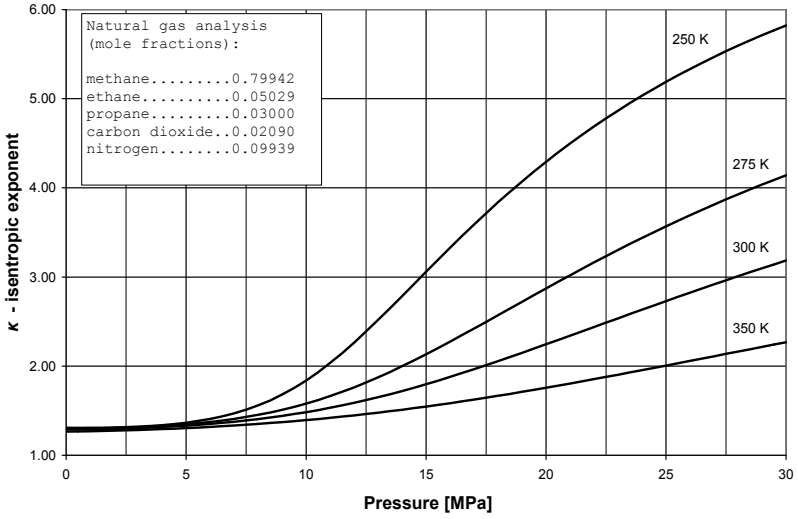

Fig. 4. Calculated isentropic exponent of the natural gas mixture.

From Table 4 it can be seen that the calculated values of μ_{JT} are within ±0.113 K/MPa with the experimental results for the pressures up to 30 MPa. The relative difference increases with the increase of pressure but never exceeds ±2.5% for the pressures up to 12 MPa. At higher pressures, when the values of μ_{JT} are close to zero, the relative difference may increase significantly. The calculation results obtained for pure methane and methane-ethane mixture are in considerably better agreement with the corresponding experimental data (Ernst et al., 2001) than for the natural gas mixture shown above. We estimate that the relative uncertainty of the calculated c_p and μ_{JT} of the AGA-8 natural gas mixtures in common industrial operating conditions (pressure range 0-12 MPa and temperature range

250-350 K) is unlikely to exceed ±3.00 % and ±4.00 %, respectively. Fig. 4 shows the results of the calculation of the isentropic exponent. Since the isentropic exponent is a theoretical parameter there exist no experimental data for its verification.

5. Flow rate measurement

Flow rate equations for differential pressure meters assume a constant fluid density of a fluid within the meter. This assumption applies only to incompressible flows. In the case of compressible flows, a correction must be made. This correction is known as adiabatic expansion factor, which depends on several parameters including differential pressure, absolute pressure, pipe inside diameter, differential device bore diameter and isentropic exponent. Isentropic exponent has a limited effect on the adiabatic correction factor but has to be calculated if accurate flow rate measurements are needed.

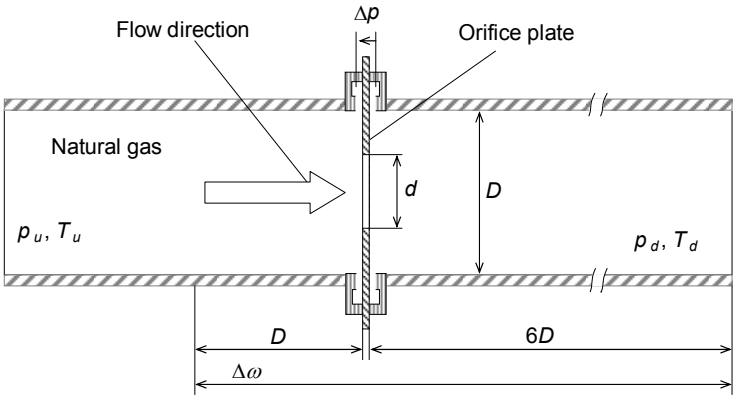

Fig. 5. The schematic diagram of the natural gas flow rate measurement using an orifice plate with corner taps.

When a gas expands through the restriction to a lower pressure it changes its temperature and density (Fig. 5). This process occurs under the conditions of constant enthalpy and is known as JT expansion (Shoemaker at al., 1996). It can also be considered as an adiabatic effect because the pressure change occurs too quickly for significant heat transfer to take place. The temperature change is related to pressure change and is characterized by the JT coefficient. The temperature change increases with the increase of the pressure drop and is proportional with the JT coefficient. According to (ISO5167, 2003) the upstream temperature is used for the calculation of flow rate but the temperature is preferably measured downstream of the differential device. The use of downstream instead of upstream temperature may cause a flow rate measurement error due to the difference in the gas density caused by the temperature change. Our objective is to derive the numerical procedure for the calculation of the natural gas specific heat capacity, isentropic exponent and JT coefficient that can be used for the compensation of flow rate error. In order to make the computationally intensive compensation procedure applicable to low computing power real-time measurement systems the low complexity surrogate models of original procedures will be derived using the computational intelligence methods: ANN and GMDH. The

surrogate models have to be tailored to meet the constraints imposed on the approximation accuracy and the complexity of the model, i.e. the execution time (ET).

6. Compensation of flow rate error

We investigated the combined effect of the JT coefficient and the isentropic exponent of a natural gas on the accuracy of flow rate measurements based on differential devices. The measurement of a natural gas (ISO-12213-2, 2006) flowing in a pipeline through orifice plate with corner taps (Fig. 5) is assumed to be completely in accordance with the international standard (ISO-5167, 2003). The detailed description of the flow rate equation with the corresponding iterative computation scheme is given in (ISO-5167, 2003). The calculation of the natural gas flow rate depends on multiple parameters:

$$q_u = q\left(P_u, T_u, \Delta p, \rho_u, \gamma_u, \kappa_u, D, d\right), \tag{40}$$

where q_u, ρ_u, γ_u and κ_u represent the corresponding mass flowrate, density, viscosity and the isentropic exponent calculated at upstream pressure P_u and temperature T_u, while D and d denote the internal diameters of the pipe and the orifice, respectively. In case of the upstream pressure and the downstream temperature measurement, as suggested by (ISO-5167, 2003), the flow rate equation, Eq. (40), changes to:

$$q_d = q\left(P_u, T_d, \Delta p, \rho_d, \gamma_d, \kappa_d, D, d\right), \tag{41}$$

where q_d, ρ_d, γ_d and κ_d denote the corresponding mass flow rate, density, viscosity and the isentropic exponent calculated in "*downstream conditions*" i.e. at the upstream pressure p_u and the downstream temperature T_d. For certain natural gas compositions and operating conditions the flow rate q_d may differ significantly from q_u and the corresponding compensation for the temperature drop effects, due to JT expansion, may be necessary in order to preserve the requested measurement accuracy (Maric & Ivek, 2010).
The flow rate correction factor K can be obtained by dividing the true flow rate q_u calculated in the upstream conditions, Eq. (40), by the flow rate q_d calculated in the "*downstream conditions*", Eq. (41):

$$K = \frac{q_u}{q_d} \tag{42}$$

For the given correction factor Eq. (42), the flow rate at the upstream pressure and temperature can be calculated directly from the flow rate computed in the "*downstream conditions*", i.e. $q_u = K \cdot q_d$. Our objective is to derive the GMDH polynomial model of the flow rate correction factor. Given the surrogate model (K_{SM}) for the flow rate correction factor Eq. (42), the true flow rate q_u can be approximated by: $q_{SM} = K_{SM} \cdot q_d$, where q_{SM} denotes the corrected flow rate.
The flow rate through orifice is proportional to the expansibility factor ε, which is related to the isentropic exponent κ (ISO-5167, 2003):

$$\varepsilon = 1 - \left(0.351 + 0.256\beta^4 + 0.93\beta^8\right) \cdot \left[1 - \left(p_d / p_u\right)^{1/\kappa}\right], \tag{43}$$

where β denotes the ratio of the diameter of the orifice to the inside diameter of the pipe, while p_u and p_d are the absolute pressures upstream and downstream of the orifice plate, respectively. The corresponding temperature change (ΔT) of the gas for the orifice plate is defined by

$$\Delta T = T_u - T_d \approx \mu_{JT}(p_u, T_d)\Delta\omega\,, \tag{44}$$

where T_u and T_d indicate the corresponding temperatures upstream and downstream of the orifice plate, $\mu_{JT}(p_u, T_d)$ is the JT coefficient at upstream pressure p_u and downstream temperature T_d and $\Delta\omega$ is the pressure loss across the orifice plate (Urner, 1997)

$$\Delta\omega = \frac{\sqrt{1-\beta^4\left(1-C^2\right)} - C\beta^2}{\sqrt{1-\beta^4\left(1-C^2\right)} + C\beta^2}\Delta p\,, \tag{45}$$

where C denotes the coefficient of discharge for orifice plate with corner taps (ISO-5167, 2003) and ΔP is the pressure drop across the orifice plate. According to (ISO-5167, 2003), the temperature of the fluid shall preferably be measured downstream of the primary device but upstream temperature is to be used for the calculation of the flow rate. Within the limits of application of the international standard ISO-5167 it is generally assumed that the temperature drop across differential device can be neglected but it is also suggested to be taken into account if higher accuracies are required. It is also assumed that the isentropic exponent can be approximated by the ratio of the specific heat capacity at constant pressure to the specific heat capacity at constant volume of ideal gas. These approximations may produce a considerable measurement error. The relative flow measurement error E_r is estimated by comparing the approximate (q_d) and the corrected (q_u) mass flow rate i.e.

$$E_r = \left(q_d - q_u\right)/q_u \tag{46}$$

Step	Description
1	Calculate the natural gas properties (ρ_d, μ_{JT} and κ_d) at p_u, and T_d, (Table 2).
2	Calculate the dynamic viscosity γ_d at P_u, and T_d, using e.g. the residual viscosity equation (Poling, 2000).
3	Calculate the mass flow rate q_d and the discharge coefficient C at P_u, T_d and Δp (ISO-5167, 2003).
4	Calculate the pressure loss $\Delta\omega$, Eq. (45).
5	Calculate the upstream temperature T_u in accordance with Eq. (44).
6	Calculate the natural gas properties (ρ_u and κ_u) at p_u, and T_u, (Table 2).
7	Calculate the dynamic viscosity γ_u at p_u, and T_u, using e.g. the residual viscosity equation (Poling, 2000).
8	Calculate the mass flow rate q_u at p_u, T_u and Δp (ISO-5167, 2003).

Table 5. Precise correction of the flow rate based on downstream temperature measurement and on the computation of natural gas properties.

The individual and the combined relative errors due to the approximations of the temperature drop and the isentropic exponent can be estimated by using the Eq. (46). The precise correction of the natural gas flow rate, based on upstream pressure and downstream temperature measurement and on the computation of the corresponding natural gas properties, is summarized in Table 5.

The procedure in Table 5 requires a double calculation of both the flow rate and the properties of the natural gas. To reduce the computational burden we aim to derive a low-complexity flow rate correction factor model that will enable direct compensation of the flow rate error caused by the measurement of the downstream temperature. The correction factor model has to be simple enough in order to be executable in real-time and accurate enough to ensure the acceptable measurement accuracy.

7. Results of flow rate measurement simulations

In order to simulate a flow rate measurement error caused by the non-compensated temperature drop, a natural gas mixture (Gas 3) from Annex C of (ISO-12213-2, 2006) is assumed to flow through orifice plate with corner taps (ISO-5167, 2003) as illustrated in Fig. 5. Following the recommendations (ISO-5167, 2003), the absolute pressure is assumed to be measured upstream (p_u) and the temperature downstream (T_d) of the primary device. Fig. 6

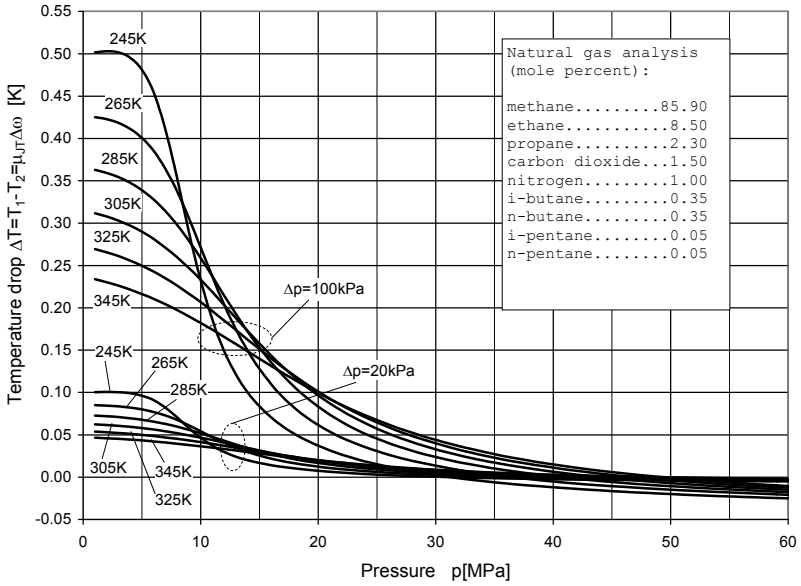

Fig. 6. Temperature drop due to JT effect $\Delta T = \mu_{JT}\Delta\omega$ when measuring flow rate of natural gas mixture through orifice plate with corner taps (ISO-5167, 2003). The upstream pressure varies from 1 MPa to 60 MPa in 1 MPa steps and upstream temperature from 245 K to 305 K in 20 K steps for each of the two differential pressures Δp (20 kPa and 100 kPa). The internal diameters of orifice and pipe are: d=120 mm and D=200 mm.

illustrates the temperature drop caused by the JT effect and calculated in accordance with the Eq. (44). The calculated results are given for two discrete differential pressures (Δp), 20kPa and 100kPa, for absolute pressure (p_u) ranging from 1 MPa to 60 MPa in 1 MPa steps and for six equidistant upstream temperatures (T_u) in the range from 245 to 345 K. From Fig. 6 it can be seen that for each temperature there exists the corresponding pressure where JT coefficient changes its sign and consequently alters the sign of the temperature change. A relative error in the flow rate measurements due to JT effect is shown in Fig. 7. The error is calculated in accordance with Eq. (46) by comparing the approximate mass flow rate (q_d) with the precisely calculated mass flow rate (q_u). The approximate flow rate and the corresponding natural gas properties (density, viscosity and isentropic exponent) are calculated at upstream pressure p_u, downstream temperature T_d and differential pressure Δp, by neglecting the temperature drop due to JT effect ($T_d = T_u$). The results are shown for two discrete differential pressures (Δp), 20kPa and 100kPa, for absolute upstream pressure (p_u) ranging from 1 MPa to 60 MPa in 1 MPa steps and for four equidistant downstream temperatures (T_d) in the range from 245 to 305 K.

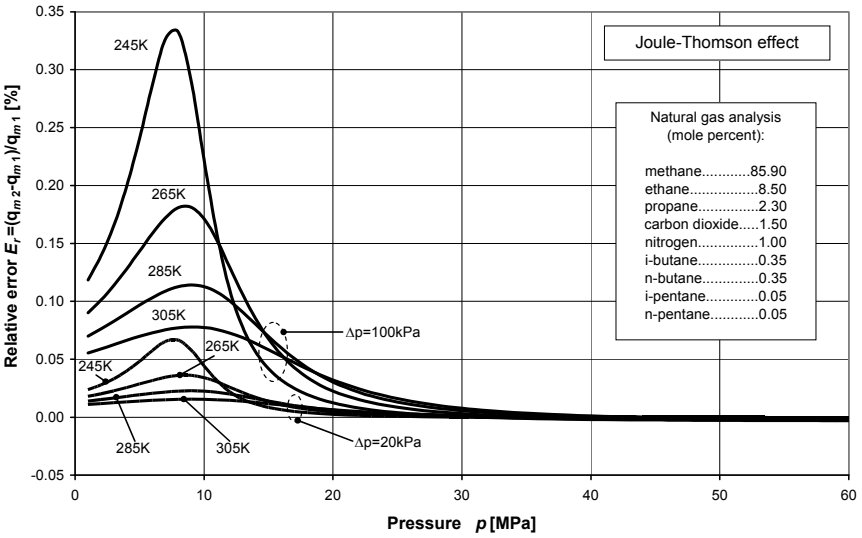

Fig. 7. Relative error $E_r = (q_d - q_u)/q_u$ in the flow rate of natural gas measured by orifice plate with corner taps (ISO-5167, 2003) when calculating flow rate using downstream temperature with no compensation of JT effect (q_d) instead of upstream temperature (q_u). The upstream pressure varies from 1 MPa to 60 MPa in 1 MPa steps and downstream temperature from 245 K to 305 K in 20 K steps for each of two differential pressures Δp (20 kPa and 100 kPa). The internal diameters of orifice and pipe are: d=120 mm and D=200 mm.

Fig. 8 illustrates the relative error in the flow rate measurements due to the approximation of the isentropic exponent by the ratio of the ideal molar heat capacities. The error is calculated by comparing the approximate mass flow rate (q_d) with the precisely calculated

mass flow rate (q_u) in accordance with Eq. (46). The procedure for the precise correction of the mass flow rate is shown in Table 5. The approximate flow rate calculation is carried out in the same way with the exception of the isentropic exponent, which equals the ratio of the ideal molar heat capacities ($\kappa = c_{m,pI} / \left(c_{m,pI} - R\right)$). The results are shown for two discrete differential pressures Δp (20kPa and 100kPa), for absolute upstream pressure p_u ranging from 1 MPa to 60 MPa in 1 MPa steps and for four equidistant downstream temperatures T_d in the range from 245 to 305 K.

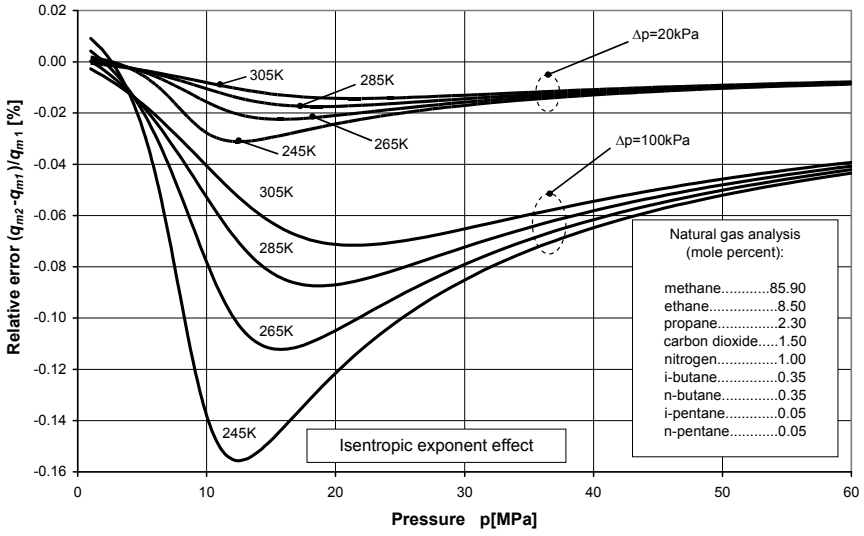

Fig. 8. Relative error $E_r = \left(q_d - q_u\right)/q_u$ in the flow rate of natural gas mixture measured by orifice plate with corner taps (ISO-5167, 2003) when using the isentropic exponent of ideal gas (q_d) instead of real gas (q_u). The upstream pressure varies from 1 MPa to 60 MPa in 1 MPa steps and downstream temperature from 245 K to 305 K in 20 K steps for each of two differential pressures Δp (20 kPa and 100 kPa). The internal diameters of orifice and pipe are: d=120 mm and D=200 mm.

Fig. 9 shows the flow rate measurement error produced by the combined effect of the JT and isentropic expansion. The error, Eq. (46), is calculated by comparing the approximate mass flow rate (q_d) with the mass flow rate (q_u) calculated precisely in accordance with the procedure depicted in Table 5. The approximate flow rate and the corresponding natural gas properties are calculated at upstream pressure p_u, downstream temperature T_d and differential pressure Δp, by neglecting the temperature drop due to JT effect ($T_d = T_u$) and by substituting the isentropic exponent by the ratio of the ideal molar heat capacities, $\kappa = c_{m,pI} / \left(c_{m,pI} - R\right)$. The results are shown for two discrete differential pressures Δp (20kPa and 100kPa), for absolute upstream pressure p_u ranging from 1 MPa to 60 MPa in 1

MPa steps and for four equidistant downstream temperatures T_d in the range from 245 to 305 K.

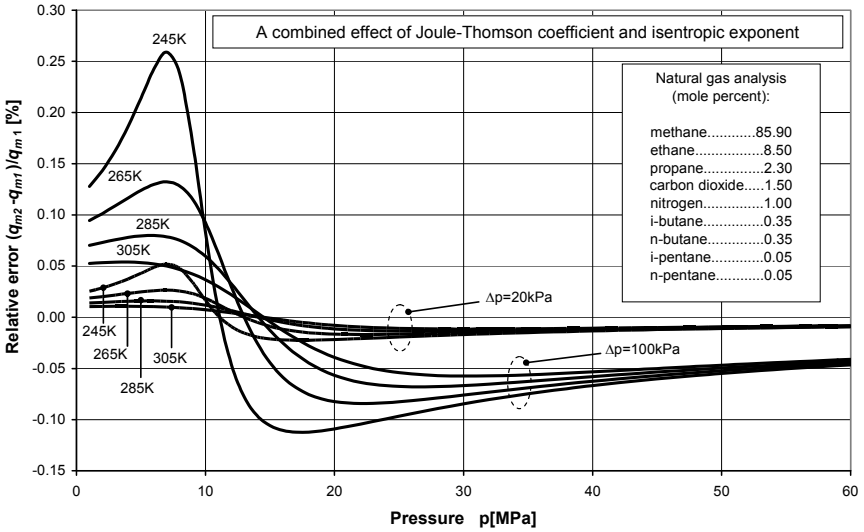

Fig. 9. Relative error $E_r = (q_d - q_u)/q_u$ in the flow rate of natural gas mixture measured by orifice plate with corner taps (ISO-5167, 2003) when using downstream temperature with no compensation of JT effect and the isentropic exponent of ideal gas at downstream temperature (q_d) instead of upstream temperature and the corresponding real gas isentropic exponent (q_u). The upstream pressure varies from 1 MPa to 60 MPa in 1 MPa steps and downstream temperature from 245 K to 305 K in 20 K steps for each of two differential pressures Δp (20 kPa and 100 kPa). The internal diameters of orifice and pipe are: d=120 mm and D=200 mm.

The results obtained for JT coefficient and isentropic exponent are in a complete agreement with the results obtained when using the procedures described in (Marić, 2005) and (Marić et al., 2005), which use a natural gas fugacity to derive the molar heat capacities. The calculation results are shown up to a pressure of 60 MPa, which lies within the wider ranges of application given in (ISO-12213-2, 2006), of 0 - 65 MPa. However, the lowest uncertainty for compressibility is for pressures up to 12 MPa and no uncertainty is quoted in reference (ISO-12213-2, 2006) for pressures above 30 MPa. Above this pressure, it would therefore seem sensible for the results of the JT and isentropic exponent calculations to be used with caution. From Fig. 9 it can be seen that the maximum combined error is lower than the maximum individual errors because the JT coefficient (Fig. 7) and the isentropic exponent (Fig. 8) show the counter effects on the flow rate error. The error always increases by decreasing the natural gas temperature. The total measurement error is still considerable especially at lower temperatures and higher differential pressures and can not be overlooked. The measurement error is also dependent on the natural gas mixture. For certain mixtures, like natural gas with high carbon dioxide content, the relative error in the flow rate may increase up to 0.5% at lower operating temperatures (245 K) and up to 1.0% at

very low operating temperatures (225 K). Whilst modern flow computers have provision for applying a JT coefficient and isentropic exponent correction to measured temperatures, this usually takes the form of a fixed value supplied by the user. Our calculations show that any initial error in choosing this value, or subsequent operational changes in temperature, pressure or gas composition, could lead to significant systematic metering errors.

8. Flow rate correction factor meta-modeling

Precise compensation of the flow rate measurement error is numerically intensive and time-consuming procedure (Table 5) requesting double calculation of the flow rate and the properties of a natural gas. In the next section it will be demonstrated how the machine learning and the computational intelligence methods can help in reducing the complexity of the calculation procedures in order to make them applicable to real-time calculations. The machine learning and the computationally intelligence are widely used in modeling the complex systems. One possible application is meta-modeling, i.e. construction of a simplified surrogate of a complex model. For the detailed description of the procedure for meta-modeling the compensation of JT effect in natural gas flow rate measurements refer to (Marić & Ivek, IEEE, Marić & Ivek, 2010).

Approximation of complex multidimensional systems by self-organizing polynomials, also known as the Group Method of Data Handling (GMDH), was introduced by A.G. Ivakhnenko (Ivaknenkho, 1971). The GMDH models are constructed by combining the low-order polynomials into multi layered polynomial networks where the coefficients of the low-order polynomials (generally 2-dimensional 2nd-order polynomials) are obtained by polynomial regression. GMDH polynomials may achieve reasonable approximation accuracy at low complexity and are simple to implement in digital computers (Marić & Ivek, 2010). Also the ANNs can be efficiently used for the approximation of complex systems (Ferrari & Stengel, 2005). The main challenges of neural network applications regarding the architecture and the complexity are analyzed recently (Wilamowski, 2009).

The GMDH and the ANN are based on learning from examples. Therefore to derive a meta-model from the original high-complexity model it is necessary to (Marić & Ivek, 2010):

- generate sufficient training and validation examples from the original model
- learn the surrogate model on training data and verify it on validation data

We tailored GMDH and ANN models for a flow-computer (FC) prototype based on low-computing-power microcontroller (8-bit/16-MHz) with embedded FP subroutines for single precision addition and multiplication having the average ET approximately equal to 50 μs and 150 μs, respectively.

8.1 GMDH model of the flow rate correction factor

For the purpose of meta-modeling the procedure for the calculation of the correction factor was implemented in high speed digital computer. The training data set, validation data set and 10 test data sets, each consisting of 20000 samples of correction factor, were randomly sampled across the entire space of application. The maximum ET of the correction factor surrogate model in our FC prototype was limited to 35 ms ($T_{exe0} \leq 35$ ms) and the maximum root relative squared error (RRSE) was set to 4% ($E_{rrs0} \leq 4\%$). Fig. 10 illustrates a polynomial graph of the best discovered GMDH surrogate model of the flow rate correction factor obtained at layer 15 when using the compound error (CE) measure (Marić & Ivek, 2010). The

RRSE (E_{rrs}=3.967%) and the ET (T_{exe}=32 ms) of the model are both below the given thresholds (E_{rrs0}=≤4.0% and T_{exe0}≤35 ms) making the model suitable for implementation in the FC prototype.

GMDH polynomial model in recursive form

$y=P_{31}(P_{30}(P_{28}(P_{27}(P_{26}(P_{25}(P_{20}(P_{19}(P_{18}(P_{17}(P_{11}(P_8(P_6(P_2(P_0(x_4,x_8),P_1(x_2,x_3)),P_5(P_3(x_3,x_4),P_4(x_6,x_7))),P_7(x_0,x_7)),P_{10}(P_9(x_0,x_4),P_1(x_2,x_3))),P_{16}(P_{15}(P_{13}(P_0(x_4,x_8),P_{12}(x_3,x_6)),P_{14}(x_2,x_5)),x_7)),P_{14}(x_2,x_5)),x_1),x_3),P_{24}(P_{22}(P_{21}(x_3,x_8),x_4),P_{23}(x_5,x_6))),x_6),P_{14}(x_2,x_5)),x_5),P_{29}(P_1(x_2,x_3),x_4)),x_3)$

Basic regression polynomial

$$P_i(z_j,z_k)=a_0(i)+a_1(i)\ z_j+a_2(i)z_k+a_3(i)\ z_jz_j+a_4(i)\ z_kz_k+a_5(i)z_jz_k$$

Coefficients of the polynomials P_0 to P_{31}

i	a_0	a_1	a_2	a_3	a_4	a_5
0	1.0001E+0	-1.1357E-2	-6.8704E-4	2.5536E-4	8.0474E-4	8.4350E-3
1	9.8856E-1	-3.3090E-4	6.7325E-5	7.0360E-6	-1.0142E-7	7.3114E-7
2	-8.1858E+2	7.4253E+2	8.9596E+2	5.0943E+1	-2.5870E+1	-8.4398E+2
3	9.9012E-1	6.6260E-5	-4.1345E-2	-1.1050E-7	-2.7501E-5	1.1208E-4
4	1.0005E+0	5.2566E-3	-1.0140E-4	-5.5278E-3	9.3191E-7	4.1835E-6
5	-4.9380E+1	-3.2481E+1	1.3133E+2	-1.5787E+1	-9.7756E+1	6.5075E+1
6	-1.6081E+2	2.4385E+2	7.9023E+1	-1.7140E+1	6.5044E+1	-2.0896E+2
7	9.9774E-1	7.4210E-3	1.0690E-4	-6.6765E-3	-1.7098E-6	-2.4801E-4
8	-1.2395E+3	1.2696E+3	1.2113E+3	-3.1377E+1	-2.2670E+0	-1.2068E+3
9	9.9999E-1	8.5310E-4	-7.3055E-3	-7.3184E-3	4.8341E-4	-1.1245E-2
10	-4.3539E+2	1.2580E+3	-3.8654E+2	-1.0374E+2	7.1916E+2	-1.0505E+3
11	6.0579E+1	-8.4832E+1	-3.5432E+1	7.7879E+1	5.2456E+1	-6.9650E+1
12	9.8649E-1	6.4671E-5	5.4189E-3	-1.0113E-7	-7.4088E-3	1.0893E-5
13	-2.5121E+2	8.1232E+2	-3.0962E+2	4.1247E+1	6.0267E+2	-8.9441E+2
14	9.9954E-1	3.3668E-4	-5.4531E-5	-1.9968E-5	-2.5227E-9	3.5061E-6
15	-2.7176E+2	3.6409E+2	1.8065E+2	1.0868E+1	1.0229E+2	-3.8514E+2
16	-6.1959E+1	1.2610E+2	-2.8801E-2	-6.3142E+1	5.4548E-7	2.8761E-2
17	-3.0692E-1	1.6415E+1	-1.4806E+1	-1.8346E+1	-2.8921E+0	2.0936E+1
18	-1.8777E+2	1.1482E+2	2.6201E+2	6.4193E+1	-9.9645E+0	-2.4228E+2
19	-7.8929E+0	1.6780E+1	1.0244E+0	-7.8875E+0	5.9509E-3	-1.0252E+0
20	1.6250E+0	-2.4087E+0	5.0903E-4	1.7861E+0	2.4507E-8	-5.2458E-4
21	9.8493E-1	7.8212E-5	3.7369E-3	-1.0339E-7	8.8817E-4	-1.2276E-5
22	-8.8257E+1	1.7868E+2	-1.0451E+1	-8.9419E+1	-2.5096E-4	1.0451E+1
23	9.9690E-1	-3.3893E-6	8.3911E-3	-3.1845E-9	-6.8053E-3	-8.7023E-7
24	-8.0245E+2	6.4401E+2	9.6266E+2	2.1901E+1	-1.3782E+2	-6.8731E+2
25	2.0536E+1	1.4721E+2	-1.8732E+2	-1.2442E+2	4.2649E+1	1.0234E+2
26	-1.1994E+1	2.4927E+1	1.3707E-1	-1.1932E+1	7.7668E-4	-1.3829E-1
27	-3.3928E+1	-4.8502E+1	1.1742E+2	-2.0110E+1	-1.0364E+2	8.9758E+1
28	3.3045E+0	-5.6009E+0	-2.2026E-4	3.2964E+0	6.1967E-9	2.1961E-4
29	5.6656E+1	-1.1139E+2	-9.6569E+0	5.5730E+1	8.1188E-4	9.6565E+0
30	7.6042E+0	8.0651E+0	-2.2283E+1	1.6229E+0	1.6282E+1	-1.0291E+1
31	1.0721E+1	-2.0678E+1	7.3476E-4	1.0958E+1	8.2460E-9	-7.4024E-4

Table 6. GMDH polynomial model of the correction factor in recursive form with the corresponding coefficients of the second order two-dimensional polynomials.

The recursive equation of the flow rate correction factor model (Fig. 10) and the corresponding coefficients of the basic polynomials, rounded to 5 most significant decimal digits, are shown in Table 6, where $x_0,...,x_8$ denote the input parameters shown in Table 7. Table 7 also specifies the ranges of application of input parameters. The detailed description of the procedure for the selection of optimal input parameters is described in (Marić & Ivek, 2010). The layers in Fig. 10 are denoted by 'L00' to 'L15' and the polynomials by '$P_m(n)$', where 'm' indicates the order in which the polynomials are to be calculated recursively and 'n' denotes the total number of the basic polynomial calculations necessary to compute the m^{th} polynomial by the corresponding recursive equation.

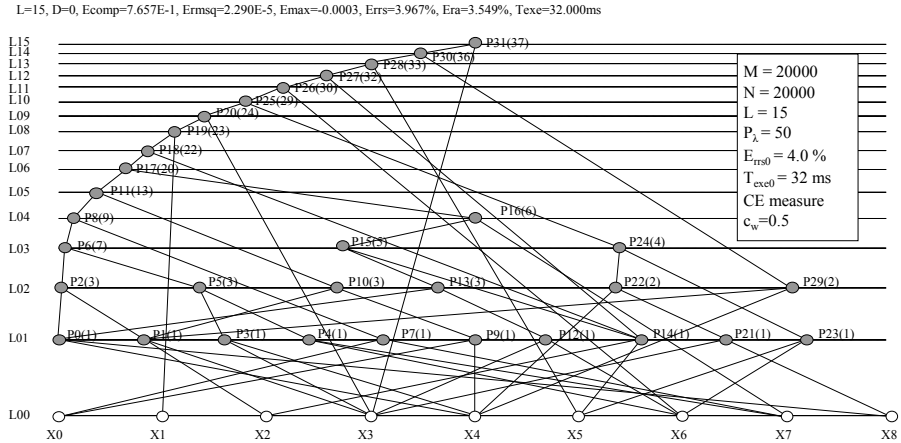

Fig. 10. Polynomial graph of the best GMDH surrogate model of the flow rate correction factor K (Marić & Ivek, 2010), obtained at layer 15 by using the CE measure with weighting coefficient c_w=0.5.

Index	Parameter description	Range of application
0	X_{CO2} - mole fraction of carbon dioxide	$0 \le X_{CO2} \le 0.20$
1	X_{H2} - mole fraction of hydrogen	$0 \le X_{H2} \le 0.10$
2	p - absolute pressure in MPa	$0 < p \le 12$
3	T - temperature in K	$263 \le T \le 368$
4	Δp - differential pressure in MPa	$0 \le \Delta p \le 0.25p$
5	ρ - density in kg/m^3	unspecified
6	ρ_r - relative density	$9.55 \le \rho_r \le 0.80$
7	H_S - superior calorific value in MJ/m^3	$30 \le H_S \le 45$
8	β - orifice to pipe diameter ratio: d/D	$0.1 \le \beta \le 0.75$

Table 7. Input parameters for the natural gas flow rate correction factor modeling.

8.2 MLP model of the flow rate correction factor

Similarly, a simple feedforward ANN the multilayer perceptron (MLP), consisting of four nodes in a hidden layer and one output node (Fig. 11), with sigmoid activation function, $\sigma = \left(1 + e^{-\sum_{i=1}^{N}(w_i x_i + b)}\right)^{-1}$, has been trained to approximate the correction factor using the same data sets and the same constraints on the RRSE and ET as in GMDH example. The output (y) from MLP, can be written in the form:

$$y = \sigma\left(b_0 + \sum_{i=1}^{4}\left(w_i \cdot \sigma\left(b_i + \sum_{j=0}^{8}\left(w_{ij} \cdot x_j\right)\right)\right)\right), \tag{47}$$

where x_j represents the j^{th} input parameter (Table 7), while b_i, w_i and w_{ij} denote the coefficients (Table 8), obtained after training the MLP by the Levenberg-Marquardt algorithm.

i	w_i	b_i	w_{0i}	w_{1i}	w_{2i}	w_{3i}
0	-	1.3996E+02	1.2540E-02	-1.9365E+00	1.6910E+00	2.8704E-01
1	-1.0130E+01	4.3451E+00	-1.7140E-02	1.1891E+00	-9.8349E-01	-2.2546E-01
2	-1.6963E+01	-3.9870E-01	8.7299E-04	3.1764E-02	-3.8641E-02	-1.3140E-02
3	-2.1044E+01	4.7731E-01	4.3873E-04	5.9977E-03	-6.8960E-03	-2.3687E-03
4	-1.0418E+02	4.0630E+00	8.1728E-02	-1.2010E+00	1.9725E+00	2.6340E+01
5	-	-	1.7424E-04	9.3751E-03	-4.0967E-03	7.4620E-04
6	-	-	-9.6008E-02	4.1284E-01	-1.7563E-01	9.0026E-02
7	-	-	-3.1605E-03	-2.5425E-02	2.6349E-02	8.6144E-03
8	-	-	-2.9468E+00	-2.1838E-02	5.6189E-02	3.6848E-02

Table 8. MLP coefficients truncated to 5 most significant digits.

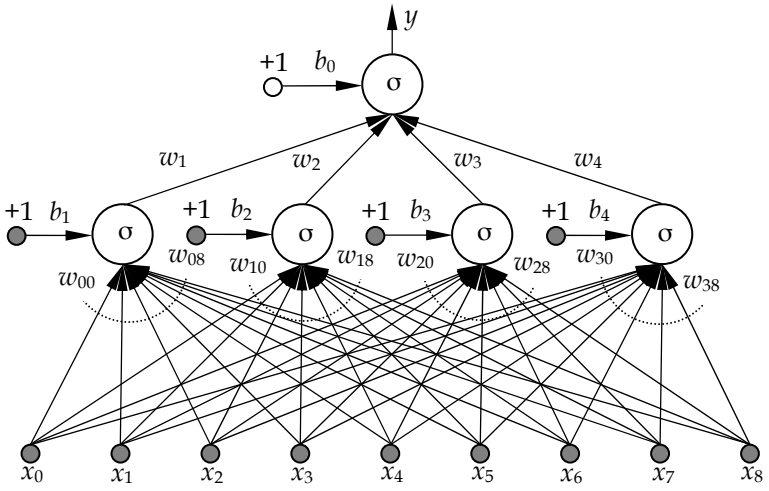

Fig. 11. MLP scheme for the flow rate correction factor modeling.

8.3 Flow rate correction error analysis

The execution times (complexities) of the MLP from Fig. 11 (T_{exe} =28 ms) and the GMDH model from Fig. 10 (T_{exe}=32 ms) are comparable but the embedding of MLP in FC software is slightly more complicated since it needs the implementation of the exponential function. The accuracy and the precision of the derived models were tested on 10 randomly generated data sets and the summary of the results is shown in Table 9. From Table 9 it can be seen that the standard deviation equals approximately 1% of the corresponding average value of RMSE and RRSE for both models and we may conclude that the derived correction factor approximates the correction procedure consistently in the entire range of application. In this particular application the MLP has significantly lower approximation error than the GMDH, both having approximately equal complexity. Note that RMSE and RRSE can be further decreased if increasing the number of layers (GMDH) or nodes (MLP) but this will also increase the corresponding execution time of the model. Fig. 12 illustrates the results of the simulation of a relative error, Eq. (46), in the measurement of a natural gas flow rate when ignoring the JT expansion effects (q_d), instead of its precise correction (q_u) in accordance with the procedure outlined in Table 5. The calculation of the flow rate is simulated by assuming the square-edged orifice plate with corner taps (ISO-5167, 2003), with orifice diameter of 20 mm, the pipe diameter of 200 mm, the differential pressure of 0.2 MPa, and with the downstream measurement of temperature. The error corresponds to the natural gas mixture 'Gas 3', given in Table G.1 of Annex G in (ISO-20765-1, 2005), which produces the largest temperature changes of all six mixtures given for validation purposes. The pressure varies from 1 MPa to 12 MPa in 0.5 MPa steps and the temperature from 263 K to 338 K in 10 K steps.

Validation set index	GMDH: E_{rms} x10^{-5}	GMDH: E_{rrs} [%]	MLP: E_{rms} x10^{-5}	MLP: E_{rrs} [%]
1	2.305	4.007	1.744	3.022
2	2.267	3.939	1.772	3.071
3	2.258	3.933	1.749	3.032
4	2.225	3.910	1.725	2.989
5	2.270	3.922	1.740	3.014
6	2.303	3.999	1.761	3.051
7	2.295	3.969	1.751	3.034
8	2.273	3.968	1.767	3.063
9	2.277	3.922	1.746	3.025
10	2.280	3.966	1.765	3.059
Mean value: $\bar{x} = \frac{1}{N}\sum_{1}^{N} x_i$	2.275	3.954	1.752	3.036
Standard deviation: $\sigma = \sqrt{\frac{N\sum_{1}^{N} x_i^{\,2} - \left(\sum_{1}^{N} x_i\right)^2}{N(N-1)}}$	0.02356	0.03341	0.01437	0.02525

Table 9. Errors in the calculated correction coefficient when approximating the precise procedure (Table 5) by the best GMDH polynomial model (Fig. 10 and Table 6) and MLP (Fig. 11 and Table 8).

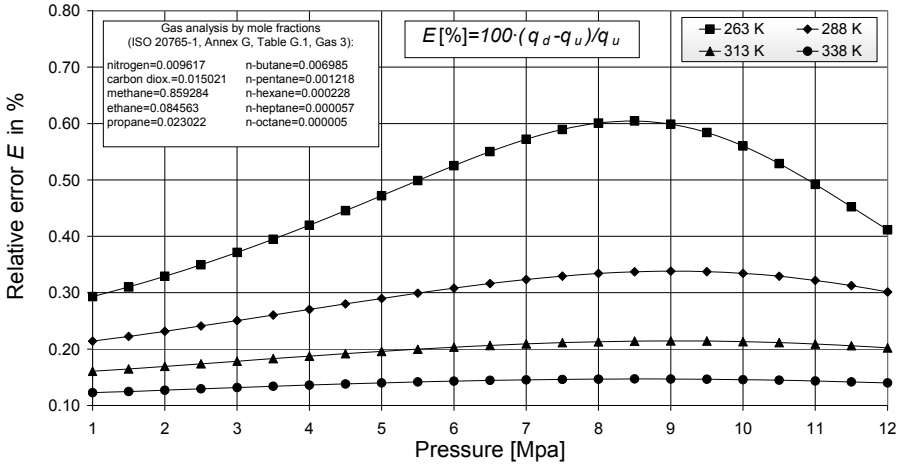

Fig. 12. Illustration of a relative error in the measurement of a natural gas flow rate by orifice plate with corner taps when ignoring the JT expansion effect.

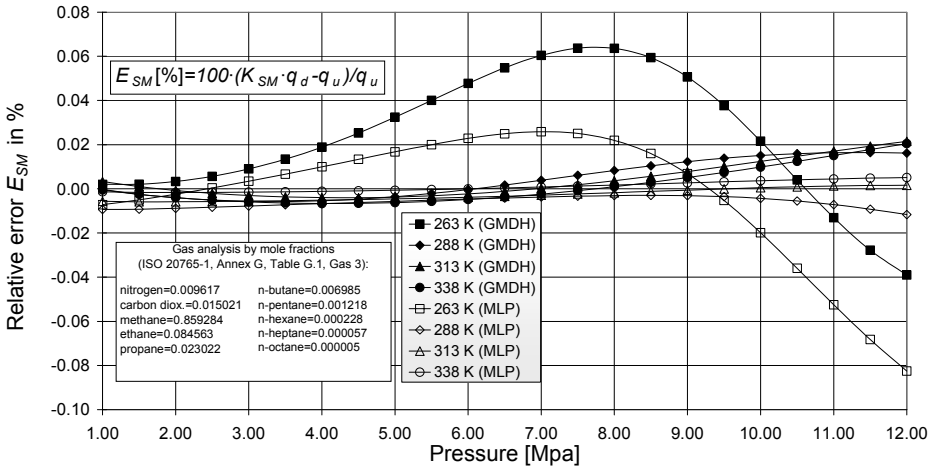

Fig. 13. Illustration of a relative error in the measurement of natural gas flow rate when using the GMDH (Fig. 10, Table 6) and MLP (Fig. 11, Table 8) surrogate models of the flow rate correction factor instead of the precise compensation procedure (Table 5).

From Fig. 12 it can be seen that the relative error slightly exceeds 0.6 % for the temperature of 263 K and for the pressures close to 8.5 MPa. The relative flow rate errors obtained for the remaining gas mixtures given in Table G.1 of (ISO-20765-1, 2005) are considerably lower.

Fig. 13 illustrates the relative flow rate error $E_{SM} = \left(K_{SM} \cdot q_d - q_u\right)/q_u$ when compensating the flow rate error by the GMDH (K_{SM}=K_{GMDH}) or by the corresponding MLP (K_{SM}=K_{MLP}), instead of its precise correction outlined in Table 5. The results in Fig. 13 are obtained by simulating the flow rate through the square-edged orifice plate with corner taps (ISO-5167,

2003), with orifice diameter of 20 mm, the pipe diameter of 200 mm, the differential pressure of 0.2 MPa, and with the downstream measurement of temperature. Again, the natural gas is taken from Table G.1 in (ISO-20765-1, 2005), and corresponds to the gas mixture denoted by 'Gas 3'. The pressure varies from 1 MPa to 12 MPa in 0.5 MPa increments and the temperature from 263 K to 338 K in 25 K increments.

From Fig. 13 it can be seen that the GMDH correction factor lowers the non-compensated relative error (Fig. 12) roughly by the order of magnitude in the entire pressure/temperature range. For the same complexity the MLP shows significantly better error performance characteristics than GMDH except at higher pressures close to 12 MPa. Both models have the error performance characteristics somewhat degraded at higher pressures and at lower temperatures but the absolute value of the relative error never exceeds 0.064% in case of GMDH and 0.083% in case of MLP. Similar results are obtained for the remaining gas mixtures from Table G.1 (ISO-20765-1, 2005) and for various randomly generated gas compositions. Almost identical error performance characteristics are obtained when applying the same GMDH model for the correction of the JT effect in the measurements using orifice plates with corner-, flange- or D&D/2-taps (ISO-5167, 2003).

The non-compensated flow rate error varies by varying the natural gas composition due to the corresponding variation of the JT coefficient. For a fixed natural gas mixture the absolute value of a JT coefficient (Marić, 2005 & 2007) is increasing by decreasing the temperature, thus increasing the temperature drop, Eq. (44), which increases the uncertainty of the calculated density of a natural gas and the uncertainty of the flow rate, as well. Also, the increase of the differential pressure and the decrease of the diameter ratio are increasing the pressure loss, Eq. (45), thus amplifying the temperature change, Eq. (44), and consequently the flow rate error.

The non-compensating flow rate error (Fig. 12) occurs when measuring the temperature downstream of the orifice plate and when assuming the same temperature upstream of the orifice plate. The procedure for the precise compensation of a temperature drop effect (Table 5) eliminates the corresponding flow rate error completely but it needs the calculation of both the flow rate and the properties of a natural gas to be executed twice and is therefore computationally intensive and time consuming and may be unacceptable for low-computing power measurement systems. The above described correction procedure performs a simple scaling of the flow rate, calculated using "downstream conditions", by the corresponding low-complexity surrogate of the correction coefficient (Eq. (42)). The correction procedure slightly increases the calculation time of a common procedure (ISO-5167, 2003) but it decreases the non-compensated flow rate error, due to the temperature drop, by one order of magnitude (Figs. 12 and 13). Most likely, the obtained surrogate models are not the best possible models. However, both derived models decrease the computational complexity of precise compensation (Table 5) significantly while preserving reasonable accuracy and are therefore applicable in low-computing-power systems. Hence, they make the error negligible with the acceptable degradation of the calculation time. For the same computational complexity the MLP surrogate of the correction procedure displays better approximation error characteristics than the GMDH model but it also exhibits slightly increased programming complexity when considering its implementation in low-computing-power microcomputer.

9. Conclusions

The above described procedure for the computation of thermodynamic properties of natural gas was originally published in the Journal Flow Measurement and Instrumentation (Marić, 2005 & 2007). The procedure is derived using fundamental thermodynamic equations (Olander, 2007), DIPPR AIChE (DIPPR® Project 801, 2005) generic ideal heat capacity equations, and AGA-8 (Starling & Savidge, 1992) extended virial-type equations of state. It specifies the calculation of specific heat capacities at a constant pressure c_p and at a constant volume c_v, the JT coefficient μ_{JT}, and the isentropic exponent κ of a natural gas. The thermodynamic properties calculated by this method are in very good agreement with the known experimental data (Ernst et al., 2001).

The effects of thermodynamic properties on the accuracy of natural gas flow rate measurements based on differential devices are analyzed. The computationally intensive procedure for the precise compensation of the flow rate error, caused by the JT expansion effects, is derived. In order to make the compensation for the flow rate error executable in real time on low-computing-power digital computers we propose the use of machine learning and the computational intelligence methods. The surrogate models of the flow rate correction procedure are derived by learning the GMDH polynomials (Marić & Ivek, 2010) and by training the MLP artificial neural network. The MLP and the GMDH surrogates significantly reduce the complexity of the compensation procedure while preserving high measurement accuracy, thus enabling the compensation of the flow rate error in real time by low-computing-power microcomputer. The same models can be equally applied for the compensation of the flow rate of natural gas measured by means of orifice plates with corner-, flange- or D and D/2-taps.

10. References

Baker, R.C. (2000). *Flow Measurement Handbook*, Cambridge University Press, ISBN: 0-521-48010-8, New York

DIPPR® Project 801, (2005). *Evaluated Process Design Data*, Design Institute for Physical Properties, Sponsored by AIChE, Electronic ISBN: 978-1-59124-881-1

Ernst, G., Keil, B., Wirbser, H. & Jaeschke, M. (2001). Flow calorimetric results for the massic heat capacity cp and Joule-Thomson coefficient of CH_4, of (0.85 CH_4 + 0.16 C_2H_6), and of a mixture similar to natural gas, *J. Chem. Thermodynamics*, Vol. 33, No. 6, June 2001, 601-613, ISSN: 0021-9614

Ferrari, S. & Stengel, R.F. (2005). Smooth Function Approximation Using Neural Networks, *IEEE Transactions on Neural Networks*, Vol. 16, No. 1, January 2005, 24-38, ISSN: 1045-9227

ISO-12213-2 (2006), *Natural gas -- Calculation of compression factor -- Part 1: Introduction and guidelines*, ISO, Ref. No. ISO-12213-2:2006(E), Geneva

ISO-20765-1, (2005), *Natural gas – Calculation of thermodynamic properties - Part1: Gas phase properties for transmission and distribution applications*, ISO, Ref. No. ISO-20765-1:2005, Geneva

ISO-5167 (2003). *Measurement of fluid flow by means of pressure differential devices inserted in circular-cross section conduits running full,* ISO, Ref. No. ISO-51671:2003(E), Geneva

Ivakhnenko, A. G. (1971). Polynomial Theory of Complex Systems, *IEEE Transactions on Systems Man, and Cybernetics*, Vol. SMC-1, No.4, Oct 1971, 364-378, ISSN: 0018-9472

Lemmon, E. W. & Starling, K. E. (2003). Speed of Sound and Related Thermodynamic Properties Calculated from the AGA Report No. 8 Detail Characterization Method Using a Helmholtz Energy Formulation, *AGA Operating Section Proceedings*, ISSN: 15535711, Phoenix, May 2004, American Gas Association.

Marić, I. & Ivek, I. (IEEE). Self-Organizing Polynomial Networks for Time-Constrained Applications, *IEEE Transactions on Industrial Electronics*, DOI: 10.1109/TIE.2010.2051934 , (accepted for publication)

Marić, I. & Ivek, I. (2010). Compensation for Joule-Thomson effect in flow rate measurements by GMDH polynomial, *Flow Measurement and Instrumentation*, Vol. 21, No. 2, June 2010, 134-142, ISSN: 0955-5986.

Marić, I. (2005). The Joule-Thomson effect in natural gas flow-rate measurements, *Flow Measurement and Instrumentation*, Vol. 16, No. 6, December 2005, 387-395, ISSN: 0955-5986

Marić, I. (2007). A procedure for the calculation of the natural gas molar heat capacity, the isentropic exponent, and the Joule-Thomson coefficient, *Flow Measurement and Instrumentation*, Vol. 18, No. 1, March 2007, 18-26, ISSN: 0955-5986

Marić, I., Galović, A. & Šmuc, T. (2005). Calculation of Natural Gas Isentropic Exponent, *Flow Measurement and Instrumentation*, Vol. 16, No. 1, March 2005, 13-20, ISSN: 0955-5986

Miller, E.W. (1996). *Flow Measurement Engineering Handbook*, McGraw-Hill, ISBN: 0-07-042366-0, New York

Nikolaev, N.Y. & Iba, H. (2003), "Learning Polynomial Feedforward Neural Networks by Genetic Programming and Backpropagation," *IEEE Transactions on Neural Networks*, Vol. 14, No. 2, March 2003, 337-350, ISSN: 1045-9227

Olander, D. R. (2007). *General Thermodynamics*, CRC Press, ISBN: 9780849374388, New York

Poling, B.E., Prausnitz, J.M. & O'Connell, J. (2000). *The Properties of Gases and Liquids*, McGraw-Hill Professional, ISBN: 0070116822, New York

Shoemaker, D.P., Garland, C.W. and Nibler, J.W. (1996). *Experiments in Physical Chemistry*, McGraw-Hill, ISBN: 9780072318210, New York

Span, R. & Wagner, W. (1996) A New Equation of State for Carbon Dioxide Covering the Fluid Region from the Triple-Point Temperature to 1100 K at Pressures up to 800 MPa, *J. Phys. Chem. Ref. Data*, Vol. 25, No. 6, November 1996, 1509-1596, ISSN 0047-2689

Span, R. & Wagner, W. (2003) Equations of State for Technical Applications. I. Simultaneously Optimized Functional Forms for Nonpolar and Polar Fluids, *Int. J. Thermophys.*, Vol. 24, No. 1, January 2003, 1-39, ISSN: 0195-928X

Starling, K. E. & Savidge, J. L. (1992). *Compressibility Factors for Natural Gas and Other Hydrocarbon Gases*, American Gas Association Transmission Measurement Committee Report No. 8, American Petroleum Institute (API) MPMS, chapter 14.2, Arlington

Urner, G. (1997), Pressure loss of orifice plates according to ISO 5167-1, *Flow Measurement and Instrumentation*, Vol. 8, No. 1, March 1997, 39-41, ISSN: 0955-5986

Wilamowski, B. M.; Cotton, N.J.; Kaynak, O. & Dündar, G. (2008). Computing Gradient Vector and Jacobian Matrix in Arbitrarily Connected Neural Networks, *IEEE Transactions on Industrial Electronics*, Vol. 55, No. 10, October 2008, 3784-3790, ISSN: 0278-0046

Wilamowski, B. M. (2009). Neural Network Architectures and Learning Algorithms, *IEEE Industrial Electronics Magazine*, Vol. 3, No. 4, December 2009, 56-63, ISSN: 1932-4529